CORROSION SCIENCE AND TECHNOLOGY, Vol.3, No.4(2004), pp.140~147

High-Temperature Oxidation of Ti Containing Stainless Steel in O_2-N_2 Atmosphere

Hidenori Onishi, Isao Saeki, Ryusaburo Furuichi, Toru Okayama*, Kenko Hanamatsu*, Tamaki Shibayama, Heishichiro Takahashi**, and Shinichi Kikkawa**

Department of Materials Science and Engineering, Graduate School of Engineering, Hokkaido University, Kita 13 Nishi 8, Sapporo, 060-8628 Japan
**Aomori Advanced Industrial Technology center, 202-4 Ashiya, Yatsuyaku, Aomori, 030-0112, Japan*
***Center for Advanced Research of Energy Technology, Hokkaido University, Kita 13 Nishi 8, Sapporo, 060-8628 Japan*

High temperature oxidation of Fe-19Cr and Fe-19Cr-0.2Ti alloys is studied at 1173-1373 K in 16.5 kPa O_2 - balances N_2 atmosphere aimed at clarifying the effect of titanium addition. Oxidation rate of Fe-19Cr alloy was accelerated with titanium. For both alloys chromium rich $(Fe, Cr)_2O_3$ was formed as a major oxidation product. On Fe-19Cr-0.2Ti alloy, a thin layer composed of spinel type oxide and titanium oxide was also formed and an internal oxidation of titanium was observed. Titanium was concentrated at the oxide surface and internal oxidation zone but a small amount of titanium was also found in the intermediate corundum type $(Fe, Cr)_2O_3$ layer. Crystals of corundum type $(Fe, Cr)_2O_3$ formed on Fe-19Cr alloy are coarse but that formed on Fe-19Cr -0.2Ti alloys were fine and columnar. Reason for the difference in oxidation kinetics and crystal structure will be discussed relating to the distribution of aliovalent titanium in corundum type $(Fe, Cr)_2O_3$ oxide layer.

Keywords : *high-temperature oxidation, titanium, stainless steel, diffusion, doping effect*

1. Introduction

It is well known that the high temperature oxidation resistance of steels and iron-base alloys is enhanced by addition of rare earth elements or so-called "active elements" whose oxygen affinities are high.[1)-3)] Preferable effects of titanium to the oxidation are also expected because oxygen affinity of titanium is strong. Many studies on high temperature oxidation of alloys and stainless steels with rare earth elements, molybdenum, niobium, and titanium have been carried out after 1970's aimed at improved oxidation resistance of thermal reactor and catalytic converter in automobile exhaustion system.[4)]

For that purpose, development of thin, light, thermal conductive, and low cost materials are required and the studies are centered on the oxidation of alumina forming Fe-Cr-Al ferrite stainless steels without expensive nickel. It was found that addition of 0.2 mass% titanium improves the oxidation resistance of Fe-Cr-Al alloys and decrease the amount of aluminum to maintain alumina film with no deteriorative effect to welding and forming properties of steels.[5)] For chromia forming Fe-Cr steels, titanium is found to beneficial as it selectively react with carbon and nitrogen in the steels and prevent embrittlement of steels due to the formation of chromium carbide or nitride.[6)] On the high temperature oxidation of chromia forming Fe-Cr steels, however, titanium was reported to increase the oxidation rate.[7)]

The opposite effect of titanium on oxidation resistance of alumina and chromia forming steels or alloys may be arose by titanium inclusion in these oxides because addition of quadvalent titanium ion may annihilate the vacancies in alumina of n-type and increase the number of vacancies in chromia of p-type semiconductors.[8)] Earlier studies using electron probe micro analyzer could not determine whether there is titanium in corundum type oxides due to spatial resolution limit,[5),9)] but recently the inclusion of titanium in chromia was confirmed.[16)] It is expected that modern analyzing methods help the establishment of the effect of titanium on the high

temperature oxidation of steels and alloys.

The objective of the present work is to compare the oxidation behavior and oxide properties between Fe-19Cr and Fe-19Cr-0.2Ti alloys and to make clear the effect of titanium. High-temperature oxidation of Fe-19Cr stainless steel with 0.2 mass% of titanium was carried out in O_2-N_2 atmosphere at 1173-1373 K. The effect of titanium on the oxidation kinetics and oxide properties will be discussed based on the results obtained by TG, XRD, SEM, GD-OES, and TEM.

2. Experimental

Laboratory forged alloys detailed in Table 1 were cut into 20x10x1 mm^3, and then they were mirror-finished with 1 μm diamond paste.

Degreased specimen was stored in a silica-gel desiccator for more than 86.4 ks before oxidation test. Specimens were heated to 1173, 1273, or 1373 K with 17 K s^{-1} and were oxidized isothermally at these temperatures. Oxidation atmosphere is adjusted to 16.5 kPa O_2 - balances N_2. Oxidation kinetics was evaluated by mass change of the specimen between before and after oxidation test. Crystal structure of oxides was analyzed by X-ray diffraction (XRD, Philips PW-3400). Surface and cross section of the specimen were observed with field-emission type secondary electron microscopes (FE-SEM, JEOL JSM-6300F or Hitachi S-4000) and a transmission electron microscope (TEM, JEOL 2000FX) after preparation with a focused ion beam facility (FIB, SMI 9200). Oxide composition was estimated by X-ray photoelectron spectroscopy (XPS, VG Escalab II) or glow discharge optical emission spectroscopy (GD-OES, HORIBA-Jovin Yvon JY5000RF).

3. Results and discussion

3.1 Oxidation kinetics

Relation between oxidation time, t_{ox}, and mass gain, ΔW, of the specimens is shown in Fig. 1. With Fe-19Cr alloy oxidized at 1173 K, $\log(\Delta W)$ increases linearly with $\log(t_{ox})$ at a slope of 1/2 indicating that the oxidation apparently follows a parabolic rate law. Similar relationship is also obtained for this alloy oxidized at 1273 and 1373 K and ΔW at the same t_{ox} increases with increasing oxidation temperature, T_{ox}. The $\log(\Delta W)$ of Fe-19Cr-0.2Ti alloy at 1173 K increases linearly with $\log(t_{ox})$ at a slope of >1/2 before ΔW <2 g m^{-2}, and then a parabolic relationship is observed. At 1273 and 1373 K, the oxidation of Fe-19Cr-0.2Ti alloy proceeds in the same manner as that at 1173 K and the breaking of lines appear at similar ΔW s. The ΔW for Fe-19Cr-0.2Ti alloy are larger than that

Table 1. Chemical composition of specimens (atomic %)

alloy	C	Si	Mn	P	S	Ni	Cr	Ti	Al	N	Fe
Fe-19Cr	0.0032	0.02	0.01	0.0018	0.0016		19.01		0.004	0.0067	bal.
Fe-19Cr-0.2Ti	0.030	0.157	0.15	0.053	0.0017	0.187	21.08	0.23	0.112	0.0263	bal.

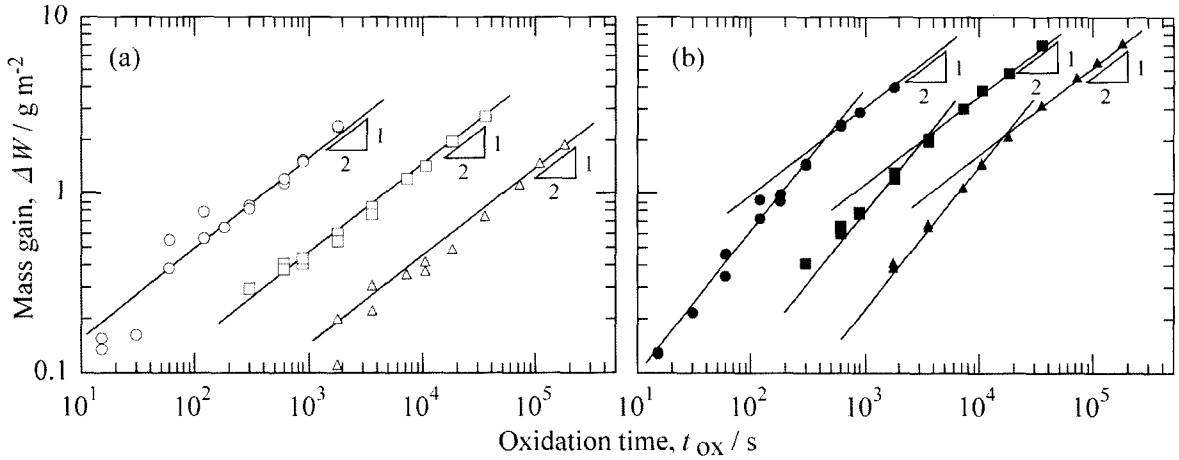

Fig. 1. Changes in mass gain with oxidation time, for (a) Fe-19Cr, (b) Fe-19Cr-0.2Ti alloys oxidized in 16.5 kPa O_2 balanced N_2 atmosphere at 1173 K (triangle), 1273 K (square), and 1373 K (circle).

of Fe-19Cr alloy in all conditions and it is clear that titanium increased oxidation rate of Fe-19Cr alloy.

3.2 Composition and crystal structure of oxide films

Fig. 2 shows typical XRD patterns of (a) Fe-19Cr and (b) Fe-19Cr-0.2Ti alloys after isothermal oxidation tests. The oxide films formed on Fe-19Cr alloy are seen to be composed of corundum type oxide in all conditions. With Fe-19Cr-0.2Ti alloy, peaks of spinel type oxide are also observed. The surface of this alloy after oxidation is rich in chromium and manganese indicating that composition of the spinel type oxide can be $(Mn,Cr)_3O_4$ where manganese occupies divalent metal ion sites.[10] In addition, a peak of TiO_2 in rutile phase appears on this alloy oxidized at 1173 K for t_{ox}>7200 and at 1273 K for t_{ox}>1800 s. Titanium was detected at the oxide surface by XPS and the TiO_2 may form there.[13]

As shown in above, the oxide films formed on both alloys are mainly composed of corundum type oxide. Lattice constant of corundum type oxide, a_c, formed at 1273 K was calculated with diffraction angles of 6 intense peaks and plotted against t_{ox} in Fig. 3. With Fe-19Cr alloy, the a_c is substantially constant independent of t_{ox}. This relation is similar to that obtained for high-temperature oxidation of Fe-16Cr stainless steels and is common for the oxide on pure Fe-Cr binary alloys.[10-12] With Fe-19Cr-0.2Ti alloy, change in a_c with t_{ox} is similar to that of Fe-19Cr alloy indicating that inclusion of titanium to the corundum type oxide is not expected or titanium content is very low.

3.3 Crystal orientation of corundum type oxides

Comparing intensity of XRD patterns between Fe-19Cr and Fe-19Cr-0.2Ti alloys, it is observed that corundum (104) peak is stronger for Fe-19Cr alloy but corundum (110) peak is stronger for Fe-19Cr-0.2Ti alloy. This indicates there is a difference in crystal orientation of corundum type oxide between alloys. Fig. 4 shows relationship between t_{ox} and crystal orientation indices of corundum type oxide, OI_{hkl}, obtained by equation 1.

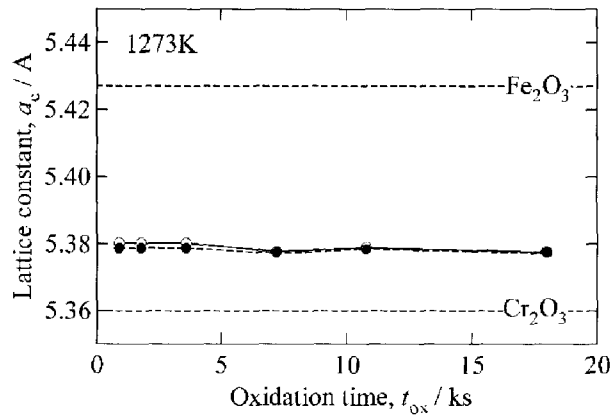

Fig. 3. Relation between oxidation time at 1273 K and lattice constants of corundum type oxides. (open marks : Fe-19Cr-0.2Ti alloy, filled marks : Fe-19Cr alloy)

$$OI_{hkl} = \left(I_{hkl}/\sum I_{hkl}\right)/\left(I_{hkl}^{JCPDS}/\sum I_{hkl}^{JCPDS}\right) \quad (1)$$

here I_{hkl} and I_{hkl}^{JCPDS} are diffraction peak heights of (hkl) planes of corundum type oxide and that of Cr_2O_3 reported in JCPDS database (38-1479). Crystal orientation can be considered to random if all OI_{hkl} equal to 1 and there is a crystal orientation if the value is larger than 1. With Fe-19Cr alloy oxidized at 1173 K, initially OI_{006}, $OI_{10\bar{1}0}$,

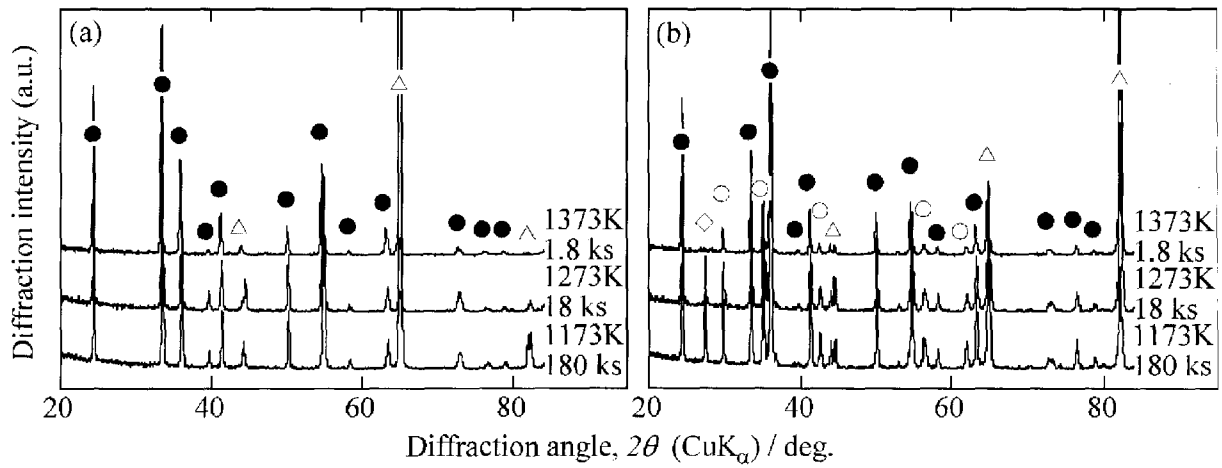

Fig. 2. XRD patterns of (a) Fe-19Cr and (b) Fe-19Cr-0.2Ti alloys after oxidation. (filled circle: Corundum type, open circle: Spinel type, triangle: substrate, diamond: Rutile)

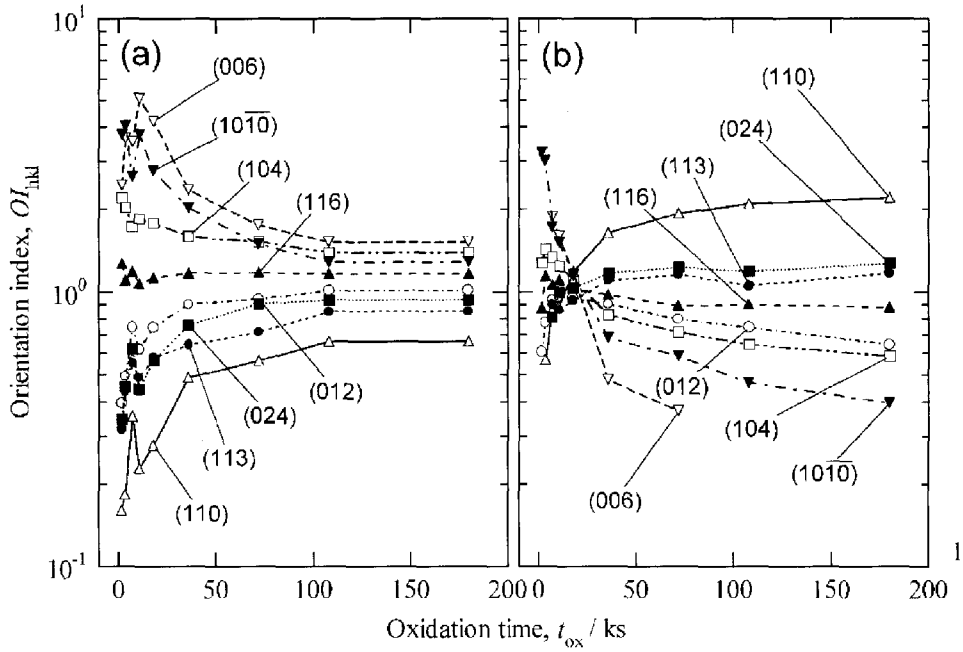

Fig. 4. Orientation indices of corundum type (Fe, Cr)$_2O_3$ oxide formed on (a) Fe-19Cr and (b) Fe-19Cr-0.2Ti alloys at 1173 K.

Table 2. Angles between basal plane of corundum type oxide (hexagonal) and crystal planes

hkl	Angle/deg.
(006)	0
(104)	15
(10$\bar{1}$0)	34
(012)	42
(116)	53
(024)	53
(113)	61
(110)	90

OI_{104}, and OI_{116} are larger and others are smaller than 1.

Orientation indices of all eight planes approach 1 with increasing t_{ox}. Similar tendency is observed for Fe-19Cr -0.2Ti alloy oxidized at T_{ox} = 1173 K at t_{ox}<18 ks. For longer oxidation time, however, OI_{110}, OI_{024}, and OI_{113} become larger than 1 and others decreases to less than 1. Angles between basal plane of corundum type oxide and crystal planes as hexagonal cell are summarized with increasing order of the angles in Table 2.

It is clear that at the initial stage of oxidation for both alloys, *OI* values for planes with smaller angle with the basal plane are large and the value decreases with increasing the angle. This indicates corundum type oxide grow preferentially to c axis of hexagonal unit cell in the initial stage. In the later oxidation stage for Fe-19Cr-0.2Ti alloy, intensities of XRD peaks for planes of higher angles with the basal plane become strong. This indicates growth to c axis direction is suppressed by titanium inclusion.

3.4 Effect of titanium on the texture of the oxide film

Fig. 5 shows cross section FE-SEM pictures of alloys oxidized at T_{ox} = 1273 K for t_{ox} = 10.8 ks and then broken in liquid nitrogen. Grains of corundum type oxide formed on Fe-19Cr alloy are large (position 1) and the oxide film is composed of one or two grain stack. Oxide film formed on Fe-19Cr-0.2Ti alloy is four times thicker than that formed on Fe-19Cr alloy and the result is coincide with mass changes in Fig. 1. Shape of the grains on this alloy is cigar shape and the long axis of them looks the surface of the oxide film (position 2). A network structure is observed beneath the corundum type oxide layer and spherical oxide particles containing titanium are observed (position 3).

Observation of oxide cross section by FE-SEM showed the difference in the shape of corundum type oxide grains but dimension of the grains could not be decided within the resolution limit of FE-SEM. Therefore, closer observation of the cross section by TEM after thinning the specimen with FIB was carried out. Fig. 6 shows TEM cross section pictures of alloys for specimens in Fig. 5. It is confirmed that large and equiaxial oxide grains are formed on Fe-19Cr alloy and cigar-shaped grains are observed on Fe-19Cr-0.2Ti alloy. Selected area diffraction

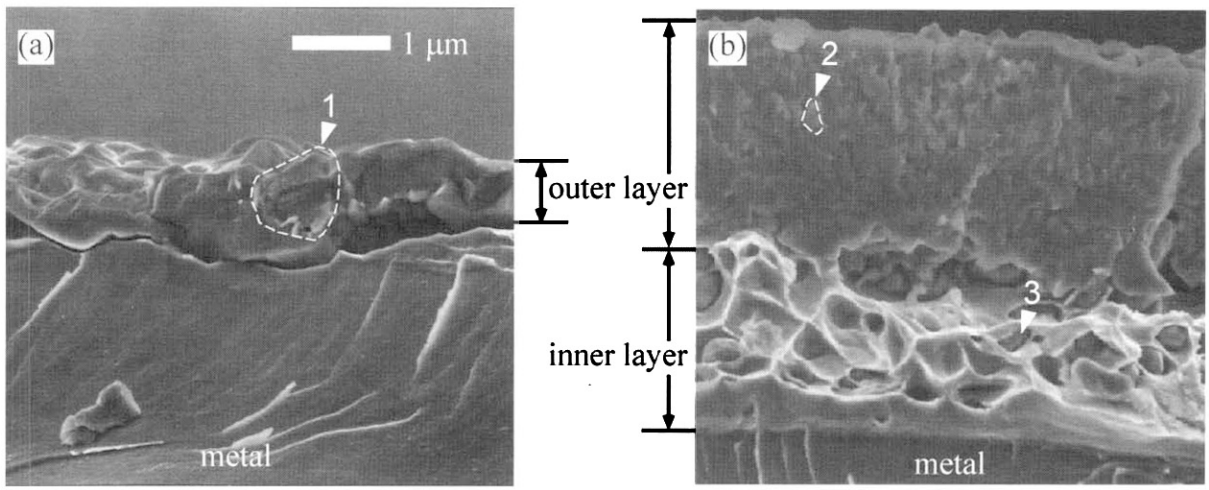

Fig. 5. SEM photographs of the oxide films formed on (a) Fe-19Cr and (b) Fe-19Cr-0.2 Ti alloys oxidized at 1273 K for 10.8 ks.

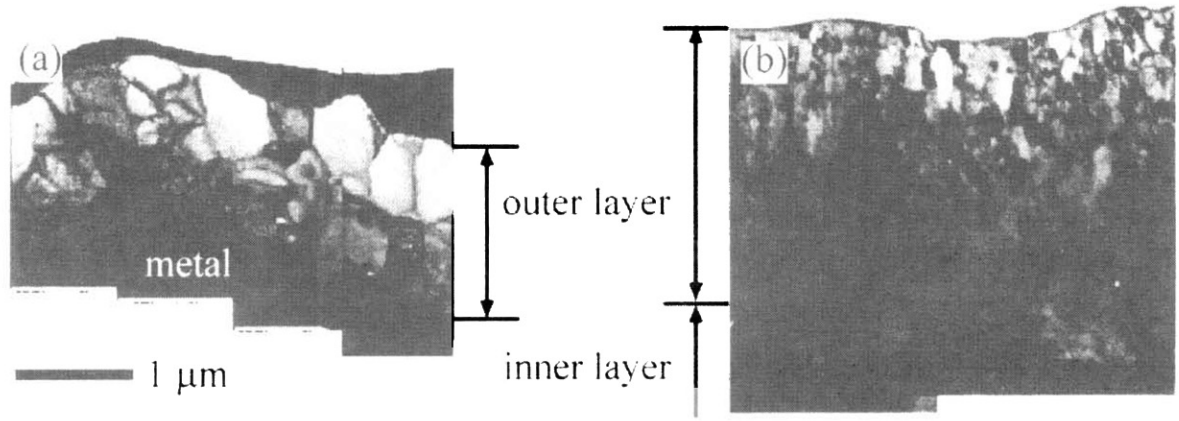

Fig. 6. TEM photographs of the oxide films formed on (a) Fe-19Cr and (b) Fe-19Cr-0.2 Ti alloys oxidized at 1273 K for 10.8 ks.

and an energy dispersive X-ray analysis combined with TEM also confirms that formed oxide layers are composed of corundum type oxide. The network texture shown in Fig. 5(b) for Fe-19Cr-0.2Ti alloy is not observed by TEM analysis indicating that the texture might form when the specimen was broken for observation. The texture, dimple pattern, clearly shows this portion is elastic at 77 K.[14)]

Dimensions of oxide grains are evaluated form TEM pictures and they are summarized in Table 3. With Fe-19Cr alloy, average length of major and minor axes are 520 and 450 nm and the ratio of them is 1.2 indicating that the formed oxide grain is equiaxial. Dimensions of cigar-shaped oxide grains formed on Fe-19Cr-0.2Ti alloy are 205 nm in major axis and 100 nm in minor axis, and the ratio of them is 2.1.

Angles between the major axis of the oxide grains and the oxide surface on Fe-19Cr alloy are evaluated and cumulative probability of them is plotted against the angle in Fig. 7. It is clear that a half of the corundum type oxide have angles larger than 65 degree and the oxide structure can be considered as columnar one. Formation of the columnar oxide layer may relate to the difference in the

Table 3. Dimensions of corundum type oxide grains formed on Fe-19Cr and Fe-19Cr-0.2Ti alloys. $\bar{L}^{maj}$ and $\bar{L}^{min}$ are average length of major and minor axis of the grains.

alloy	Fe-19Cr	Fe-19Cr-0.2Ti
$\bar{L}^{maj}$ / mm	520	205
$\bar{L}^{min}$ / mm	450	100
$\bar{L}^{maj}$ / $\bar{L}^{min}$	1.2	2.1

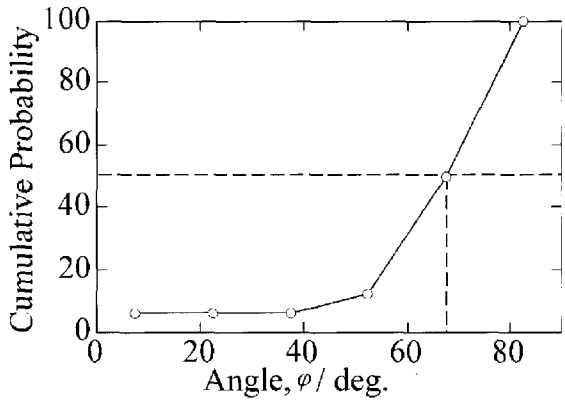

Fig. 7. Cumulative probability of the angle between major axis of oxide grains and specimen surface.

Table 4. Parabolic rate constants of Fe-19Cr and Fe-19Cr-0.2Ti alloys estimated by oxidation curves in Fig. 1.

Temp/K	$k_p \times 10^{-13}/g^2cm^{-4}s^{-1}$	
	Fe-19Cr	Fe-19Cr-2Ti
1173	1.63	29.0
1273	19	134
1373	260	920

crystal orientation shown in Fig. 3 and the minor axis of the grains is supposed to parallel to the c axis of hexagonal unit cell.

In summary, with closer observation and analysis by FE-SEM and TEM a schematic representation of corundum type oxide can be drawn as in Fig. 8. The number of oxide grain boundaries per unit length of oxide metal interface is large for Fe-19Cr-0.2Ti alloy and this may be a reason for faster oxidation rate of this alloy (Table 4).

3.5 Oxidation mechanism of titanium containing stainless steel

In the previous sections, formation of rutile type TiO_2 near the oxide surface on Fe-19Cr-0.2Ti alloys at 1173 and 1273 K was found. This indicates titanium diffuses to the oxide surface through corundum type oxide layer. X-ray emission spectra taken with TEM observation did not show the existence of titanium in corundum type oxide layer. In addition, depth profile analysis by XPS with an argon ion sputter gun could not distinguish whether titanium is in the corundum oxide layer because of low sensitivity for titanium. Therefore the authors employed GD-OES with the high sensitivity for depth profiling purpose.[15]

Fig. 9 shows results of GD-OES analysis for Fe-19Cr-0.2Ti alloys oxidized for 300, 600, and 1800 s at 1273 K. With the alloy oxidized for 300 s (a), chromium content in the oxide layer is high and iron content is low. These results coincide with the results by XRD shown in Fig. 3. Manganese is detected near the oxide surface and it may form a spinel type oxide in this region in Fig. 9(a).[10] Accumulation of titanium is observed at the oxide surface and interface between oxide and substrate alloy. Titanium is also detected between the accumulated regions and the result confirms titanium migration through corundum type oxide layer. Atomic fraction of titanium near the oxide surface increases and that in the interior of

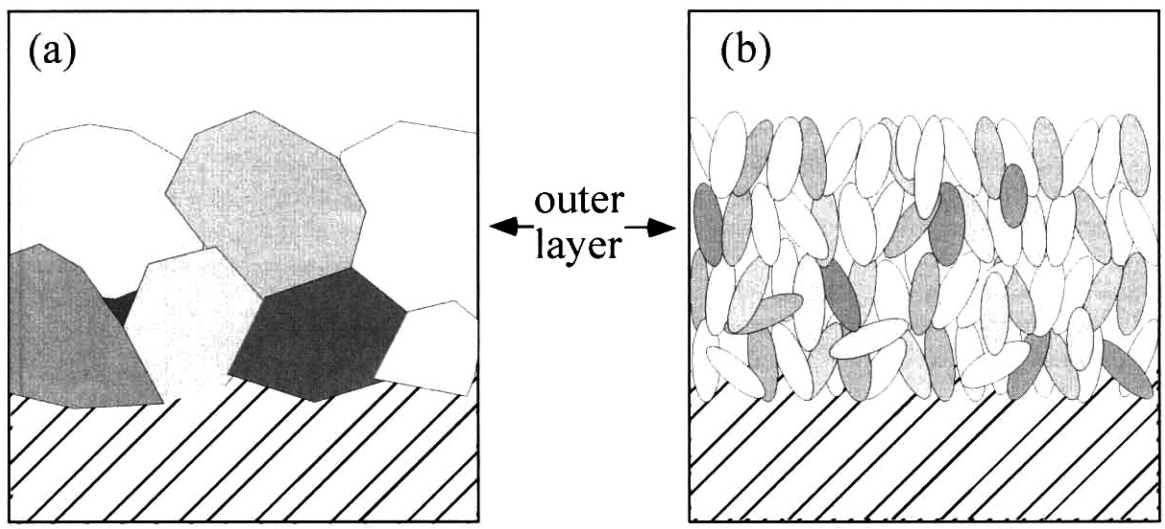

Fig. 8. Schematic representation of the structure of outer oxide layer formed on (a) Fe-19Cr, (b) Fe-19Cr-0.2Ti alloys at 1273 K in 16.5 kPa O_2 bal. N_2 for 10.8 ks.

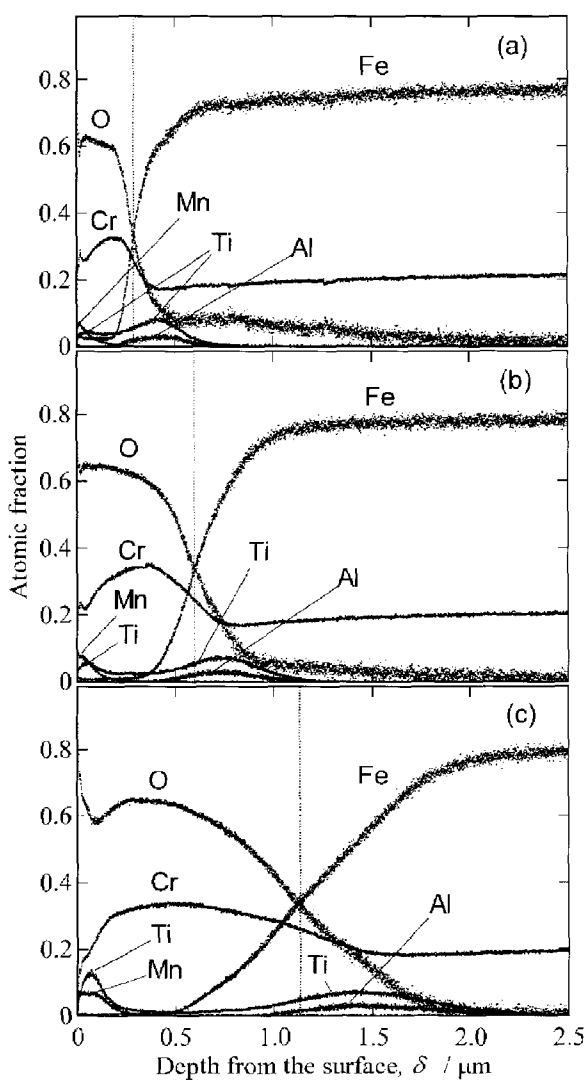

Fig. 9. Compositional depth profiles by GD-OES of Fe-19Cr-0.2Ti alloys oxidized for (a) 300 s, (b) 600 s, (c) 1800 s in 16.5 kPa 0_2 bal. N_2 atmosphere.

corundum type oxide ($\delta = 0.5$ μm in (c)) decreases with increasing oxidation time. This results indicate that fast diffusion of titanium through corundum type oxide layer do occur even though the number of diffusing titanium ion is lower than that of chromium ion. Valence of titanium ion coexisting with a large number of chromium oxides is supposed to 4. The quadvalent titanium is hard to dissolve to corundum type oxide and the titanium in the oxide layer may be segregated at the oxide grain boundaries.[17)-19)]

According to the experimental results, mechanism of the accelerated oxidation by titanium may be considered to (1) doping effect and (2) pinning effect. In mechanism (1), doping of titanium ion with the valence higher than corundum oxide matrix increases the number of cation vacancy leading to an increased cation migration rate.[20), 21)] Nagai et. al found that oxidation rate of Fe-20Cr alloy is not affected by titanium oxide dispersed in alloy substrate. In the study, titanium was not found in the oxide layer and the result may support an accelerated oxidation rate by doping mechanism.[22)] If this mechanism is generally applied to high temperature oxidation of ferrite steels and alloys, decreased oxidation rate of alumina forming alloys with titanium may be explained because alumina is n-type semiconductor and doping of cation with valence higher than 3 can decrease the number of vacancies. However, inclusion of titanium in alumina is not confirmed and further studies are necessary.[5)]

In mechanism (2), titanium ion segregated to the grain boundaries of corundum type oxide pins the movement of grain boundaries or defects leading to formation of a large number of fine oxide particles and grain boundaries in which cations migrate faster than in the oxide lattice.[23)] The authors would like to stress that this model could be proposed owing to closer observation of oxides by TEM. The present study could not decide which mechanism is predominant but one or both of the above mechanisms should explain the accelerated oxidation.

4. Conclusions

High temperature oxidation of Fe-19Cr and Fe-19Cr-0.2Ti alloys was carried out at 1173-1373 K in 16.5 kPa O_2 - balances N_2 atmosphere and the following conclusions are obtained.

(1) Corundum type oxide was the major oxidation product for both alloys. Spinel type oxide and titanium oxide were also formed near the surface of Fe-19Cr-0.2Ti alloy as well as internal oxidation of titanium was observed.

(2) Addition of titanium to Fe-19Cr alloy accelerates oxidation rate. The oxide film formed on titanium containing alloy was fine and columnar corundum type oxide. Reason for the modification of grain shape is considered to be the pinning of grain boundary motion by segregated titanium ion with valence higher than chromium ion.

(3) An accelerated oxidation by titanium addition may be explained by an increased grain boundary area or by increased cation vacancies due to doping effect of titanium with higher valence, if the grain boundary diffusion of cation is rate-limiting process.

Acknowledgements

The authors would like to acknowledge to Mr. Y. Uchida in Horiba Co. for GD-OES measurements. A part

of this study is supported by Grant-in-aid for Scientific Research of Ministry of Education, Science, and Sports, Japan (12650705), KAWASAKI STEEL 21st Century Foundation, and foundation for study on steels ISIJ.

References

1. D. P. Moon, *Mater. Sci. Technol.*, **5**, 754 (1989).
2. T. N. Rhys-Jones, H. J. Grabke, and J. Kudielka, *Corros. Sci*, **27**, 49 (1987).
3. A. Saito, I. Saeki, and R. Furuichi, *Tetsu-to-Hagane*, **85**, 30 (1999) *in Japanese.*
4. S. Ota, *Feraitotainetsuko*, p.139, Chijin Syokan, 1997, *in Japanese.*
5. S. Kado, T. Yamazaki, M. Yamanaka, K. Yoshida, K. Yabe, T. Sakamoto, Y. Nakagawa, H. Nakamura, and T. Okada, *Tetsu-to-Hagane*, **63**, 164 (1977) *in Japanese.*
6. H. Fujikawa, *Tetsu-to-Hagane*, **70**, 41 (1984) *in Japanese.*
7. H. Okabe and T. Ike, *Japan Institute of Metals*, **44**, 254 (1980) *in Japanese.*
8. P. Kofstad, High Temperature Corrosion, p.51, Elsevier, 1988.
9. O. Kobayashi and Y. Fujiwara, *Zairyo-to-Kankyo*, **43**, 640 (1994) *in Japanese.*
10. I. Saeki, H. Konno, and R. Furuichi, *Corros. Sci.*, **38**, 1595 (1996).
11. P. E. Wretblad, *Z. Anorg. Allg. Chem.*, **189**, 329 (1930).
12. I. Saeki, H. Konno, and R. Furuichi, Corros. Sci., **38**, 19 (1996).
13. Y. Kobayashi and Y. Fujiwara, Jpn. J. Corr. Eng., **43**, 640 (1996) *in Japanese.*
14. K. Kuroki, Kinzoku-no-kyodo-to-hakai, p.44, Morikita Syuppan, 1986, *in Japanese.*
15. R. Payling, *Spectroscopy*, **13**, 6 (1998).
16. M. H. Lagrange, A. M. Huntz, and J. H. Davidson, *Corros. Sci.*, **24**, 613 (1984).
17. O. Kubaschewski, C. B. Alcock, and P. J. Spencer, Materials Thermo-Chemistry, 6th Ed., p.19, Pergamon Press, 1993.
18. C. W. Lee, *Ver. Dtsh. Keram. Ges.*, **47**, 169 (1970).
19. W. D. Callister, *J. Am. Ceram. Soc.*, **62**, 208 (1979).
20. H. J. Grabke, *Surf. Interf. Anal.*, **30**, 208 (2000).
21. C. Wagner, *J. Electrochem. Soc.*, **99**, 369 (1952).
22. H. Nagai, Y. Takebayashi, and H. Mitani, *Metall. Trans*, **12A**, 435 (1981).
23. N. Nadaud, D. Kim, and Ph. Boch, *J. Am. Ceram. Soc.*, **80**, 1208 (1997).